POLITECNICO
MILANO 1863

SCUOLA DI INGEGNERIA INDUSTRIALE
E DELL'INFORMAZIONE

EXECUTIVE SUMMARY OF THE THESIS

HALOGEN BONDING IN 2D HYBRID HALIDE PEROVSKITES – Synthesis, Structural Characterization and Photophysical Properties

TESI MAGISTRALE IN MATERIALS ENGINEERING AND NANOTECHNOLOGY – INGEGNERIA DEI MATERIALI E DELLE NANOTECNOLOGIE

AUTHOR: ALESSANDRA PANIZZA

SUPERVISOR: GABRIELLA CAVALLO

ACADEMIC YEAR: 2020-2021

Introduction

Hybrid organic inorganic halide perovskites (HOIHPs) are a class of materials with the general formula ABX_3, where A is an organic cation, B a metal cation - typically Pb^{2+}, but also Sn^{2+} or Ge^{2+} have been applied to neutralize the environmental impact of Pb - and X a halide anion (I^-, Br^- or Cl^-). Their easy and low-cost production, together with their unique optoelectronic properties, make them competitive semiconductors for application in photovoltaics and optoelectronic devices (LEDs, LASERs, FETs). However, several drawbacks still hinder their practical implementation in the real world. In fact, due to their ionic nature, HOIHPs are quite sensitive to environmental factors (H_2O, O_2, temperature, light), and defects in the crystal lattice, typically undercoordinated species, behave as traps for charge carriers, limiting the stability and the efficiency of the device, respectively. The ideal crystal structure of perovskite is cubic (Fig. 1), made of a network of corner-sharing BX_6 octahedra and A cations occupying the cuboctahedral cavities. However, precise ionic size constraints dictate the stability of this cubic structure. In particular, the tolerance factor (eq. 1)

$$t = \frac{R_A + R_X}{\sqrt{2}(R_B + R_X)} \quad (1)$$

regulates the reciprocal size of the three ions (R_A, R_B, R_X radii). It is required to be in the range 0.813-1.107 for cubic structure stability,[1] thus it limits the choice of organic cation typically to MA ($CH_3NH_3^+$) and FA ($CH(NH_2)_2^+$). With larger organic cations (t > 1.11), low dimensional perovskites (2D, 1D and 0D) can be obtained. 2D HOIHPs are characterized by the alternation of monolayers of inorganic octahedra and sheets of

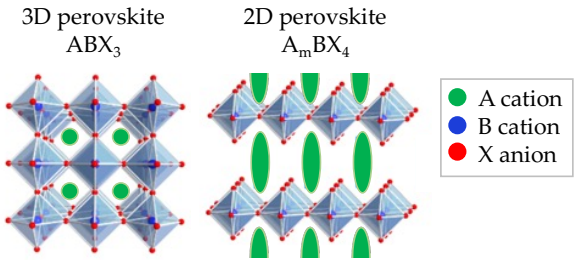

Figure 1. *Ideal cubic structure of 3D HOIP and layered structure of 2D HOIP.*[2]

organic cations (Fig. 1), resulting in formula A_2BX_4 (in case of A mono-cation). This structure confers to 2D HOIHPs a higher environmental stability than 3D HOIHPs, thanks to the hydrophobic organic cations constituting a barrier for H_2O. Moreover, the quantum confinement effect, the wide energy gap tunability and the lower volatility of organic cations open up new possibilities for application in optoelectronics. However, the quantum confinement necessarily results in a lower carrier mobility and severe charge recombination, which need to be addressed for stable and efficient devices. A smart strategy for these achievements is interaction engineering, meaning the exploitation of functionalized molecular entities, able to be involved in specific non-covalent (NC) interactions, in order to strengthen the lattice network and to passivate the undercoordinated species.[3] NC interactions, in fact, play an important role in regulating ordering, packing and optoelectronic properties of perovskites mitigating halide anion migration and segregation. Among the panel of NC interactions, halogen bond (XB) - i.*e.* the NC interaction involving halogen atoms as electrophilic sites (Fig. 2) - has proved to be a powerful tool for designing functional materials, thanks to its directionality, tunability and hydrophobicity.

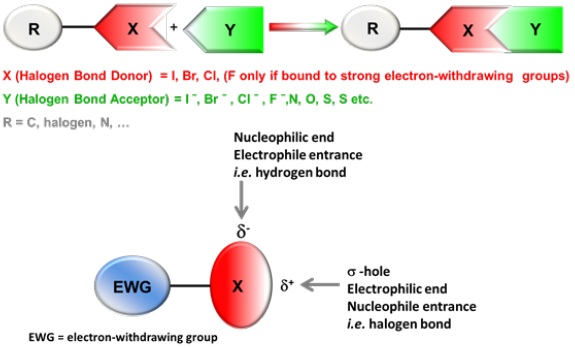

Figure 2. *Schematic representation of halogen bond (top) and the anisotropic distribution of electron density in covalently bound halogen atoms (bottom).*[4]

The interaction strength increases by increasing the electron density on Y (anions are better XB-acceptors than neutral species) and decreasing the electron density on X, therefore the presence of electron-withdrawing substituents about X, like F atoms, contribute to create stronger interactions. Recent studies reported the efficacy of XB in improving the performances of perovskites solar cells, reducing surface trap states, meliorating crystallization and film morphology and increasing the stability. Moreover, XB-donor cations have been used as templates leading to 2D HOIHP.[5] Nevertheless, an atomic/molecular understanding is highly needed for fully exploiting the advantages of XB. This work focused on the exploration of new XB-donor cations (Fig. 3) for the construction of 2D HOIHPs. The obtained materials have been characterized by FT-IR and Raman spectroscopies, XPS, XRD and SS-NMR to obtain an in-depth understanding of structure-properties relationship and dynamic processes.

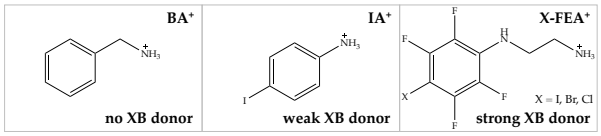

Figure 3. *Schematic representation of the cations.*

Results and Discussion

Material Design. Several XB-donor cations with tunable XB-donor ability have been selected taking into account that the main feature enabling the formation of XB is the presence of a σ-hole, *i.e.* an area of positive electrostatic potential on halogen surface, focused along the extension of the covalent bond (Fig. 2). The magnitude of the σ-hole defines the XB interaction strength and intensifies increasing the polarizability of the halogen and/or introducing electron-withdrawing substituents in the molecular scaffold. Based on this, 4-iodoanilinium (IA^+) and (4-X-2,3,5,6-tetrafluoroaniline)-ethan-1-ammonium (X-FEA^+, X = Cl, Br and I) have been applied. The first is expected to be the weakest XB-donor, while X-FEA^+, due to ring fluorination, are stronger XB-donor. We also prepared, as a model compound, a perovskite containing benzylammonium (BA^+).

Synthesis. Cations were synthesized upon reaction between the correspondent amines and HI. X-FEA amines were obtained by reacting ethylendiamine with X-pentafluorobenzene (X = Cl, Br, I), while BA and IA are commercially available and were used as received. Amines and cations were characterized by ^1H, ^{13}C and ^{19}F NMR and MS, which proved their purity. Perovskites were then obtained by mixing the cation and PbI_2 in 3:1 molar ratio in aqueous HI solution (57% wt) and purified by crystallization. Good-quality single crystals suitable for X-ray analysis were obtained only for perovskite containing IA^+ cations (Fig. 4).

Characterization. SC-XRD showed a 2D layered structure, corresponding to $(IA)_2PbI_4$ molecular formula, with corner-sharing PbI_6 octahedra layers alternated to IA^+ sheets. The presence of a weak XB was confirmed by measuring I···I^- distance, resulting to be 3.904 Å, only 3.4% shorter than the sum of VdW radii. The C-I···I^- bond angle of 163.38°, quite far from linearity, further corroborates the weakness of the interaction. $(IA)_2PbI_4$ structure was compared with $(XA)_2PbI_4$ analogues reported in literature (X = Br, Cl) to find some property trends related to XB strength. As expected, the X···I^- distance increases (XB strength decreases) in the order I < Br < Cl according to the cation XB-donor ability, which enhances with the polarizability of X. The distance between two adjacent inorganic sheets was also measured, getting slightly increasing values in the order ClA^+ (3.783 Å) < BrA^+ (3.862 Å) < IA^+ (3.904 Å). This suggests that the layers move apart increasing the cation size. This interlayer distance

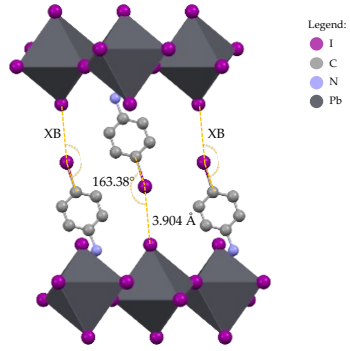

Figure 4. *Crystalline structure of $(IA)_2(PbI_4)$ highlighting XB length and angle. H atoms are omitted for clarity.*

trend is clearly visible also in XRPD simulated spectra shift (Fig. 5). In particular, the first main isolated peak, associated to (00l) planes, undergoes a shift toward lower values of 2θ, confirming the sheets distancing for heavier X atom. To classify $(XA)_2PbI_4$, other parameters were extrapolated from crystal structures. Tolerance factors were calculated according to eq.

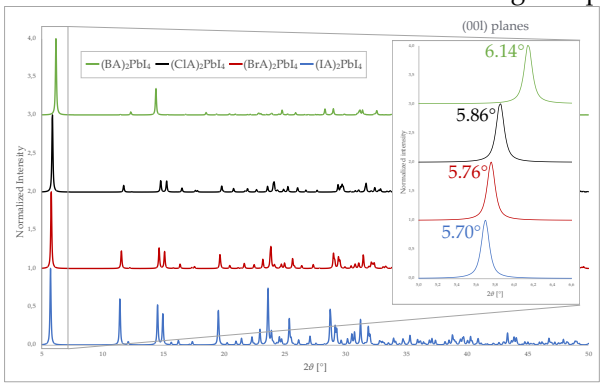

Figure 5. *Simulated XRPD patterns of $(BA)_2PbI_4$ and $(XA)_2PbI_4$, with zoom on peaks correspondent to (00l) planes.*

(1), obtaining all values higher than 1.11, as expected for low dimensional perovskites. Taking into account the offsets (*x*,*y*) between two adjacent inorganic sheets, being ~(1/3,1/3), it was possible to label the three structures as near-RP (Ruddlesden-Popper) 2D HOIHPs, considering the ideal configurations being RP for (1/2,1/2) and DJ (Dion-Jacobson) for (0,0), (0,1/2) or (1/2,0) offsets (Fig. 6). Distortion parameters, among which penetration depth, Pb-I-Pb bond angle and

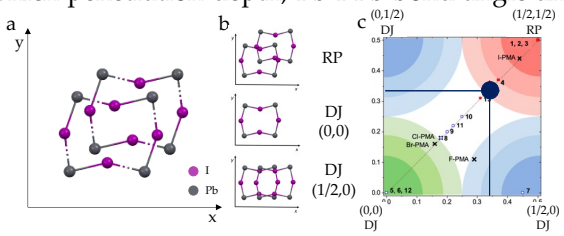

Figure 6. *Offset between two inorganic sheets (a) of $(IA)_2(PbI_4)$ and (b) of ideal configurations. (c) Graph showing how (1/3,1/3) offset (blue dot) can be classified as near-RP structure.*

out-of-plane distortion, were additionally measured, allowing to calculate the bond length quadratic elongation ⟨λ⟩ and bond angle variance σ^2 as in eqs. (2) and (3):

$$\langle\lambda\rangle = \frac{1}{6}\sum_{i=1}^{6}\left(\frac{d_i}{d_0}\right)^2 \quad (2)$$

$$\sigma^2 = \frac{1}{11}\sum_{i=1}^{12}(\alpha_i - 90)^2 \quad (3)$$

being d_i the Pb-I bond lengths, d_0 the Pb–I bond length for a regular octahedron of the same volume and α_i the I–Pb–I bond angles, and obtaining a decreasing structural distortion in the order Cl > Br > I. TGA confirmed the expected stoichiometry, being the organic phase (~40%) the first to decompose at about 120°C. From DSC, T_{deg} resulted to be 143°C, without any recognizable phase transition in the range -50° - 200°C. Vibrational spectroscopy is another useful technique to probe the occurrence of XB. In fact, the presence of XB interaction between molecules is always accompanied by the changes of IR and Raman spectra of complex relative to that of each molecule. Usually, upon XB interaction, the signal associated to C-X stretching mode of the XB-donor undergo a red-shift - the stronger the interaction, the greater the shift. In case of IA derivatives (IAI and $(IA)_2PbI_4$), the red shift is not significant with respect to amine, in accordance with the weakness of the interaction established. SC-XRD allowed to obtain crystalline structure of I-FEA amine, which already exhibited a strong XB interaction between I and N atoms (~20% shorter than the sum of VdW radii), as shown in Fig. 7.

.

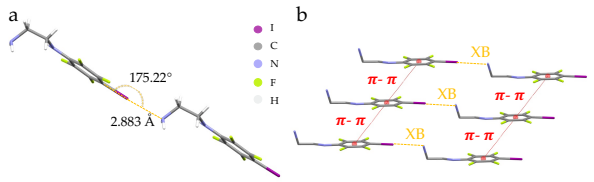

Figure 7. *I-FEA crystalline structure, highlighting (a) XB length and angle and (b) main interactions determining the arrangement.*

Since it was not possible to obtain good-quality single crystals for perovskite containing X-FEA$^+$, they were first characterized by XRPD. XRPD spectra showed a pattern similar to $(IA)_2PbI_4$ with an intense peak at low angles which can be associated to (00l) planes. This suggests a 2D structure (Fig. 8) and a chemical formula (I-FEA)$_2$PbI$_4$. This peak is at lower angles

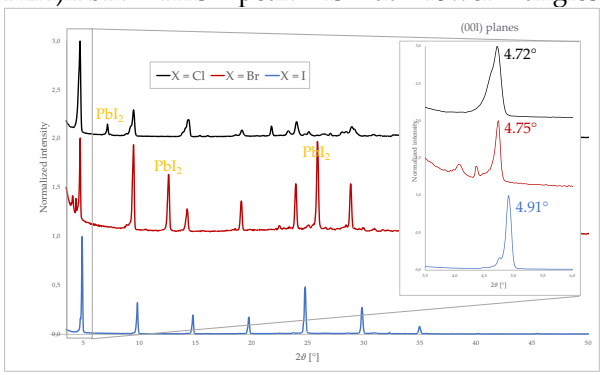

Figure 8. *Experimental XRPD patterns of (X-FEA)$_2$PbI$_4$, with some peaks associated to PbI$_2$ excess and zoom on (00l) planes peaks.*

with respect to $(BA)_2PbI_4$ and $(XA)_2PbI_4$ and it suggests that inorganic sheets move apart in the order $(BA)_2PbI_4$ < $(XA)_2PbI_4$ < (X-FEA)$_2$PbI$_4$. This trend can be easily explained taking into account the sizes of cations, which increase in the order BA^+ < XA^+ < X-FEA$^+$. However, looking at (X-FEA)$_2$PbI$_4$, it emerged that the (00l) peak shifts at higher values going from Cl-FEA$^+$, to Br-FEA$^+$ and I-FEA$^+$. This means that, increasing the size of X (and consequently of the cation), parallel inorganic sheets get closer to each other. This trend, counterintuitive if considering only cation size, can be explained assuming that the cation is involved in XB with the inorganic layer and this interaction becomes stronger by increasing the polarizability (and the size) of X. I-FEA$^+$ is the biggest cation, but it is also able to form the strongest XB, and this affects perovskite structure. TGA and DSC allowed to investigate thermal properties of the three perovskites, verifying the expected stoichiometries and obtaining T_{deg} around 300°C, slightly increasing in the order Cl < Br < I, following the XB strengthening. XPS has been also applied to investigate the XB in (I-FEA)$_2$PbI$_4$. The XPS spectrum of perovskite showed a doublet at 620.1 eV/631.6 eV corresponding to binding energy (E_b) for I 3d orbitals. This doublet accounts for the presence of different iodine species (I^-, I covalently bound to the aromatic ring and I connecting PbI_6 octahedra, which are not all equivalent). By deconvolution, we were able to identify the I-C from organic cations at 622.1 and 633.6 eV (red dotted lines in Fig. 9a). The deconvoluted spectrum of I-FEA$^+$ shows that the same iodine is at 621.5 and 633.0 eV, while in the amine it is at 621.8 and 633.2 eV. These shifts can be correlated to the strength of the interactions involving such iodine and suggest the following trend for E_b: salt < amine < perovskite. Concerning Raman spectroscopy (Fig. 9b), I-PFB precursor was first analyzed, finding C-I stretching mode at 205 cm^{-1}. The correspondent signal in amine and salt was found at 182 cm^{-1} and 190 cm^{-1}, respectively. Due to the complex structure (Pb-I str.) found at low wave numbers in

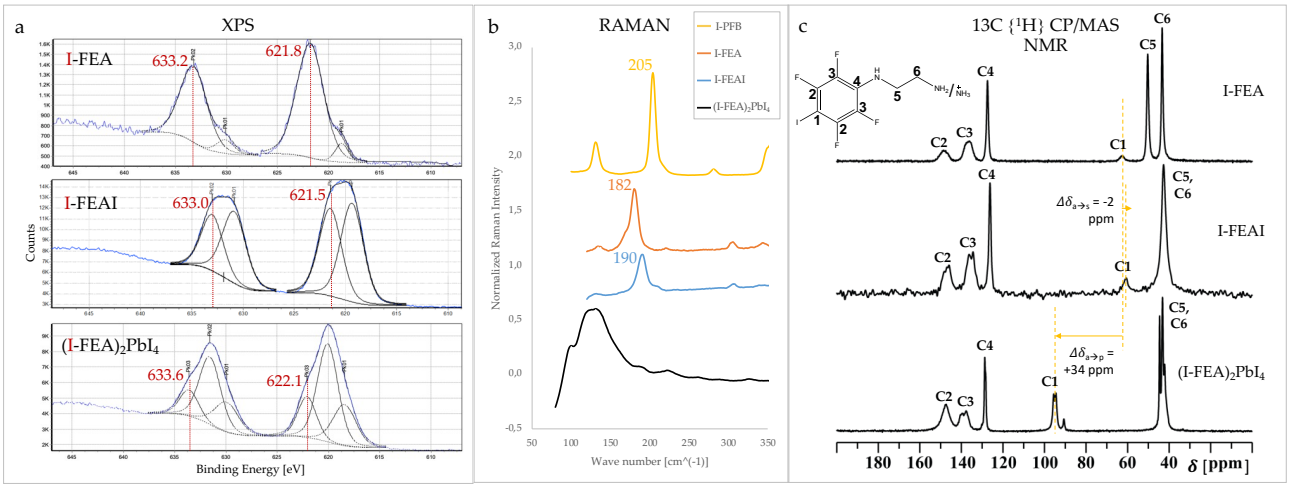

Figure 9. *Various comparative analyses among I-PFB derivatives: (a) XPS spectra, highlighting in red E_b referred to I species in organic cations; (b) Raman spectra, with labels on C-I stretching mode signals; (c) ^{13}C {^1H} CP/MAS NMR spectra, highlighting in yellow $\Delta\delta$ of C1.*

perovskite, the identification of C-I str. signal was helped by the comparison with the other 2D perovskites and PbI_2, concluding that it was red-shifted with respect to the precursor, thus suggesting a weakening of C-I bond due to the involvement of I in intermolecular interaction. This is a further proof of XB occurrence in fluorinated perovskite. SS-NMR results also contributed to support the previously observed trend, by showing an up-field shift of **C1** in salt and a down-field shift in perovskite, both with respect to amine (Fig. 9c). In addition, C atoms from the alkyl chains were identified with two well-separated signals, while they overlapped in case of salt and perovskite, probably due to the effect of protonation of the amino group, which caused an up-field shift of **C5**. NMR spectrum of $(I\text{-}FEA)_2PbI_4$ was also compared with those of its halogen-substituted analogues (Fig. 10). In particular, **C1**, seen at 103 ppm for Cl-FEA, shows an up-field shift decreasing the electronegativity of X. This carbon is the most affected by XB, therefore Δδ between **C1** of X-FEA amines and corresponding perovskites were measured to have information about the interaction strength.

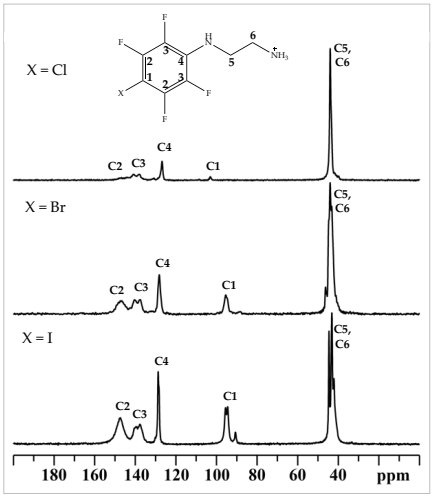

Figure 10. *^{13}C {^1H} CP/MAS SS-NMR of $(X\text{-}FEA)_2PbI_4$.*

The expected trend of XB strengthening by enhancing the polarizability of X was confirmed, finding a Δδ of 8 ppm for Cl, 15 ppm for Br and 34 ppm for I. Moreover, the exceptionally high intensity of aromatic C peaks, especially in $(I\text{-}FEA)_2PbI_4$, allowed to make some hypothesis about perovskite structure. Cations within the inorganic layers behave as bidentate ligands, with the ammonium moiety interacting with an inorganic sheet and the XB-donor group interacting through XB with the parallel inorganic sheet. Probably, cations are arranged in an antiparallel manner, such that one aromatic ring sees the alkyl chain of adjacent cations and receive magnetization from H. In this configuration the aromatic ring is "free" to rotate, and the system behaves as a supramolecular rotor. The enhanced rotational mobility is reflected on the higher intensity of NMR signals in $(I\text{-}FEA)_2PbI_4$. In view of the possible application in optoelectronic field, optical properties were investigated, trying to correlate them with structural properties. UV-vis absorption and PL measurements were conducted on all 2D synthesized perovskites. All samples resulted to have a step-like absorption spectrum (Fig. 11a), with energy gaps in the range 2.00-2.25 eV and with a quite broad dual band emission at the edge of absorption in the range ~500-600 nm (Fig. 11b). They represent the emission of lead iodide octahedra layers. In all cases, the two components of these dual PL bands differed of ~25 nm and were attributed to the different emission of surface and bulk phases. A trend in position of PL peaks can be observed, recognizing a red-shift in the order $(IA)_2PbI_4$ < $(I\text{-}FEA)_2PbI_4$ < $(BA)_2PbI_4$ < $(Cl\text{-}FEA)_2PbI_4$ < $(Br\text{-}FEA)_2PbI_4$. The shift in PL spectrum was previously identified with the different offsets among the inorganic planes. Applying the same idea to this series of

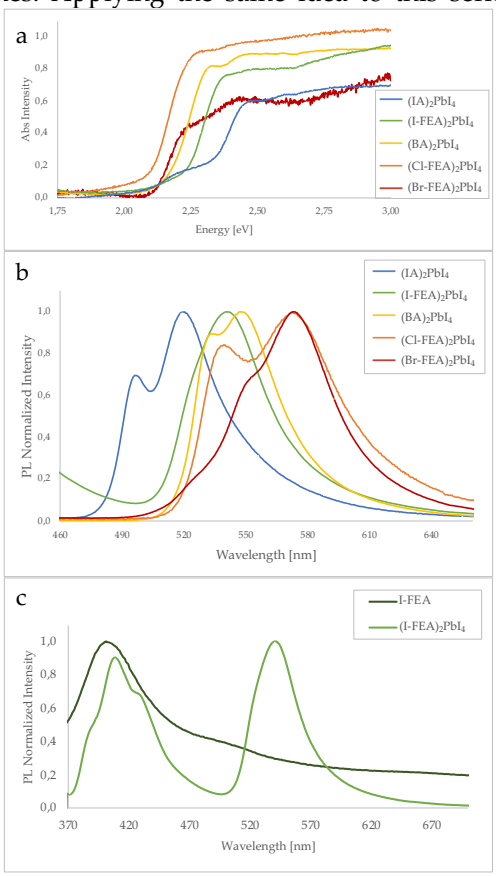

Figure 11. *(a) Absorbance and (b) steady-state PL spectra comparison among all 2D synthesized perovskites. (c) Steady state PL spectra comparison between $(I\text{-}FEA)_2PbI_4$ and I-FEA.*

2D perovskites, and starting from the well-known $(BA)_2PbI_4$ and solved-structure $(IA)_2PbI_4$, it was possible to suppose that $(I\text{-}FEA)_2PbI_4$ has an intermediate value of offset with $x = y$ (Fig. 6c), thus it is comprised between (1/3,1/3) and ideal (1/2,1/2) offsets, classifying as nRP structure. Since $(Cl\text{-}FEA)_2PbI_4$ and $(Br\text{-}FEA)_2PbI_4$ are even more red-shifted than $(BA)_2PbI_4$, they may have different offsets along x and y axes. Anomalously, steady-state PL spectrum of $(I\text{-}FEA)_2PbI_4$ presented a second band peaked at 410 nm (Fig. 11c), suggesting unusual peculiarities for this sample. From theoretical considerations and comparison with PL of I-FEA, the more energetic triple component appearing in $(I\text{-}FEA)_2PbI_4$ PL spectrum was assigned to the $\pi \rightarrow \pi^*$ transition within the aromatic rings in the cations. The emission of organic phase rarely emerges at RT, while its intensity increases upon cooling, which allows the suppression of the vibrational relaxation of the excited state electrons to the ground state *via* non-radiative internal conversion. It means that, in this perovskite, the cations are somehow constrained such that vibrational relaxation is inhibited and does not compete with radiative quenching mechanisms at RT, probably in relation to the high intensity of organic-inorganic XB interaction.

Conclusions and Outlook

Novel 2D perovskites containing XB-donor cations with different XB-donor ability have been synthesized and characterized. $(IA)_2PbI_4$ was found to exhibit a very weak XB interaction, while fluorinated cations led to stronger interactions observed through XRD, vibrational spectroscopy, XPS and NMR. These experiments collectively indicated an increasing XB intensity in the order I-FEAI < I-FEA < $(I\text{-}FEA)_2PbI_4$. While, among $(X\text{-}FEA)_2PbI_4$, the interaction strength enhances by increasing the polarizability of X. SS-NMR allowed to make some hypotheses about perovskite structure: it seems that cations inside $(I\text{-}FEA)_2PbI_4$ could act as molecular rotors. The anomalous behavior in PL emission matched the exceptional results of NMR, supporting the possibility of rotational dynamics. The hypothesis should be further investigated by ^1H spin-lattice relaxation experiments (T_1), while synchrotron would be essential for a more complete structure understanding.

Experimental Details

General synthesis of powder amines. X-FEA amines were synthesized by stirring a mixture of ethylenediamine and X-pentafluorobenzene (X-PFB) in 2:1 molar ratio for 24h at RT. The white sticky compound obtained was purified first by extractions with chloroform and water, to eliminate the excess of ethylenediamine, and then by chromatographic column, to remove unreacted traces of X-PFB, obtaining white powders.

General synthesis of powder salts. Amine (dissolved in minimum of methanol if solid) was added to hydrogen iodide (HI) water-based solution (57% wt.) in stoichiometric amount for X-FEAI, while HI was in excess for BAI and IAI. The solids precipitated immediately when HI was in excess, while in case of stoichiometric ratio the reaction was favored by concentrating the solution. After the precipitation of white solid powders, they were washed several times with diethyl ether, filtered and dried.

General synthesis of powder perovskites. PbI_2 was dissolved in HI (57% wt.) by heating and stirring. At 100°C, amine (dissolved in minimum of methanol if solid) was injected in the same flask in 3:1 molar ratio. The reaction immediately occurred, with the precipitation of a yellow/orange powder, but it was left at reflux for 45' to increase the yield. The solids were slowly (8h) cooled to RT. The crystalline powder was washed several times with diethyl ether, filtered and dried.

General synthesis of single crystals. Single crystals of amines formed spontaneously during slow drying in rotovap, before obtaining powder after complete drying. Single crystals of salts formed at initial steps of slower precipitation in more diluted methanol-based precursor solution. Perovskites single crystals were obtained through slow diffusion crystallization method.

References

1. Kim, H. S. *et al.* Organolead halide perovskite: New horizons in solar cell research. *J. Phys. Chem. C* **118**, 5615–5625 (2014).
2. Mao, L. *et al.* Two-Dimensional Hybrid Halide Perovskites: Principles and Promises. *J. Am. Chem. Soc.* **141**, 1171–1190 (2019).
3. Zhu, M. *et al.* Interaction engineering in organic-inorganic hybrid perovskite solar cells. *Mater. Horizons* **7**, 2208–2236 (2020).
4. Cavallo, G. *et al.* The halogen bond. *Chem. Rev.* **116**, 2478–2601 (2016).
5. Metrangolo, P. *et al.* Halogen Bonding in Perovskite Solar Cells: A New Tool for Improving Solar Energy Conversion. *Angew. Chemie* (2021).

Acknowledgements

This work was fulfilled thanks to the valuable contributions of Profs. S. Bracco and S. Brovelli from UniMib, Dr. M. Schiavoni from UniMi, Profs. G. Terraneo, M. M. S. Tommasini and A. Lucotti from Polimi. Grateful acknowledgments to the supervisor Prof. G. Cavallo and to all the other members of SBNlab.